Materials Transactions, Vol. 56, No. 9 (2015) pp. 1416 to 1418
Special Issue on Nanostructured Functional Materials and Their Applications

Judd–Ofelt Analysis of Eu^{3+} Emission in TiO_2 Anatase Nanoparticles

Mikhail G. Brik[1,2,3,4,*], Željka M. Antić[5], Katarina Vuković[5] and Miroslav D. Dramićanin[5]

[1]*College of Sciences, Chongqing University of Posts and Telecommunications, Chongqing 400065, P. R. China*
[2]*Institute of Physics, University of Tartu, Tartu 50411, Estonia*
[3]*Institute of Physics, Jan Dlugosz University, PL-42200 Czestochowa, Poland*
[4]*Institute of Physics, Polish Academy of Sciences, al. Lotników 32/46, 02-668 Warsaw, Poland*
[5]*University of Belgrade, Vinča Institute of Nuclear Sciences, P.O. Box 522, Belgrade 11001, Serbia*

Preparation and spectroscopic studies of the TiO_2 nanopowders doped with Eu^{3+} ions are described. Efficient emission in the red part of the visible spectrum can be obtained due to the $^5D_0 \rightarrow {}^7F_2$ emission of europium ions. Quantum efficiency of such emission was estimated to be about 0.83, which indicates a rather weak role of the non-radiative losses. However, the increase of Eu^{3+} concentration up to 10 at% significantly lowers the quantum efficiency because of the energy transfer and re-absorption processes. Higher doping concentrations (larger than 3 at% of Eu^{3+}) also decrease the covalency of the Eu^{3+}–O^{2-} chemical bonds. [doi:10.2320/matertrans.MA201566]

(Received February 27, 2015; Accepted April 6, 2015; Published June 5, 2015)

Keywords: *Judd-Ofelt analysis, TiO_2, nanoparticles, phosphorescence, europium*

1. Introduction

Titanium dioxide (TiO_2) is one of the most important metal-oxide semiconductors used for many applications including photocatalysis,[1,2] heterogeneous catalysis,[3,4] solar cells,[5] production of hydrogen, ceramics, electric devices, as well as white pigment, corrosion-protective coatings, gas sensors[6] etc. Its three natural mineral forms — anatase, rutile and brookite — are characterized with a wide energy band gaps (3.25 eV, 3.0 eV and 1.9 eV, respectively), large refractive indexes (2.488, 2.609 and 2.583, respectively) and rather low average phonon energy ($< 700\,cm^{-1}$). These properties favor doping of TiO_2 with various rare earth (RE) impurities for realizing efficient phosphorescence emissions in the visible spectral range.[7–14] Being non-toxic and biocompatible, RE doped TiO_2 is suitable for use in the bio-medical applications as a phosphorescent marker.[15] Recently, Eu^{3+} and Sm^{3+} doped anatase nanoparticles demonstrated high sensitivities in the self-referenced luminescence nano-thermometry.[16,17]

Although much work is reported on the luminescence of the RE ions in TiO_2 nanoparticles in recent times, no data on the radiative transition rates, emission branching and efficiencies of emission of RE impurities can be found. These important emission characteristics are needed to compare luminescence performance of the RE ions in TiO_2 with their performance in other, well established hosts. Therefore, we aimed in this work at an analysis of the Eu^{3+} ions emission in the prepared samples. In addition to the experimental studies, the Judd-Ofelt analysis of the emission spectra of Eu^{3+} ions was performed, which allowed to evaluate the radiative lifetimes and, as a final result, the quantum efficiency of the Eu^{3+} emission in the TiO_2 nanoparticles.

2. Experimental Details

Eu^{3+} doped anatase TiO_2 nanocrystals were prepared using the hydrolytic sol-gel route described in details elsewhere.[12] The X-ray diffraction (XRD) powder patterns were recorded using Rigaku SmartLab instrument under the Cu $K\alpha_{1,2}$ radiation. The intensity of diffraction was measured with continuous scanning at 2°/min. Transmission electron microscopy (TEM) was performed using a JEOL JEM-2100 LaB6 instrument operated at 200 kV. Photoluminescence spectra are measured with the Fluorolog-3 Model FL3-221 spectrofluorimeter system (Horiba-JobinYvon). Emission spectra were recorded under continuous excitation from a 450 W Xenon lamp at a wavelength of 360 nm and corrected to the sensitivity of the detector (PMT R928 – Horiba).

3. Results and Discussion

3.1 Microstructure and photoluminescence

The TEM image, Fig. 1(a), reveals morphology of powder of TiO_2 nanoparticles doped with 1 at% of Eu^{3+}. The powder consists of well-crystallized, loosely agglomerated nanoparticles with irregular shapes and dimensions of about 10 nm in diameter. The XRD pattern of the same sample is shown in Fig. 1(b). Diffraction peaks are indexed according to the JCPDS card No. 21-1272 (TiO_2 anatase phase, tetragonal structure, space group $I4_1/amd$ (No. 141)). Traces of rutile or brookite phase are not detected.

Figure 2 shows emission spectra of TiO_2 anatase nanoparticles doped with different nominal concentrations of Eu^{3+} (0.1; 0.5; 1; 3; 5; 7 and 10 at%) obtained with excitation at 360 nm. The spectra are composed of the spectral bands that arise from the spin-forbidden inter-shell f–f electron transitions of Eu^{3+} ions from the excited level $^5D_0$ to the ground state multiplets ($^7F_0$, $^7F_1$, $^7F_2$, and $^7F_3$ and $^7F_4$). According to our previous study,[12] emission spectra are dominated by the emission of Eu^{3+} ions located in the low-symmetry crystal site (C_1). This type of site can be related to some distorted sites near nanoparticle's surface or other defects.

3.2 Judd-Ofelt calculations and results

The Judd-Ofelt theory[18,19] was shown to be a powerful tool for an analysis of the f-f absorption spectra of trivalent lanthanides, estimations of the radiative lifetimes and

*Corresponding author, E-mail: mikhail.brik@ut.ee

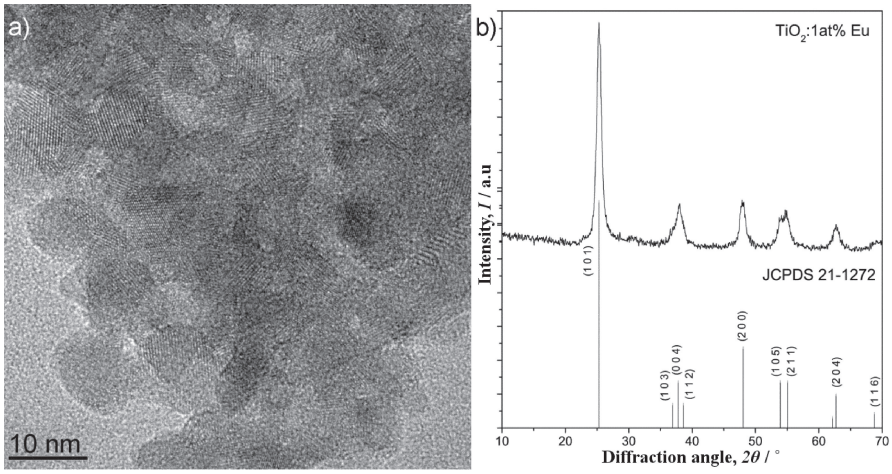

Fig. 1 Microstructure of the powder of TiO_2 nanoparticles doped with 1 at% of Eu^{3+}: (a) TEM image, (b) XRD pattern.

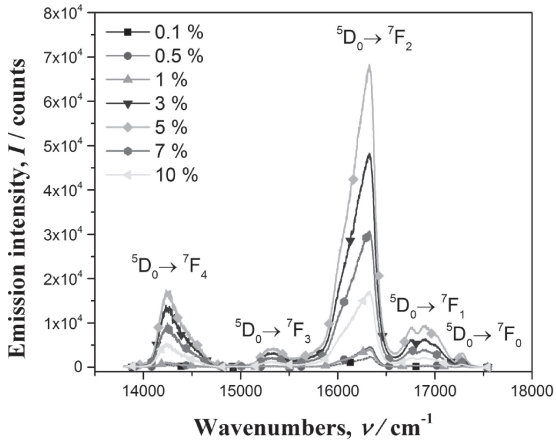

Fig. 2 Emission spectra of TiO_2 nanoparticles doped with different nominal concentrations of Eu^{3+} (0.1; 0.5; 1; 3; 5; 7 and 10 at%). The spectra were recorded under 360 nm excitation and corrected to the sensitivity of detector.

branching ratios of the emission transitions. The Eu^{3+} ion with its $4f^6$-electron shell is a very special case, because a few matrix elements of the unit tensor operators between the wave functions of this electron configuration are not zero. Due to this particular feature, one can use the Eu^{3+} emission spectra to evaluate two Judd-Ofelt intensity parameters Ω_2 and Ω_4. It is possible then to express the ratio of the radiative transition probabilities A_R of the ${}^5D_0 \rightarrow {}^7F_J$ ($J = 1, 2, 4$) transitions in terms of the ratio of areas S under corresponding emission peaks:[20,21]

$$\frac{A_R({}^5D_0 \rightarrow {}^7F_{2,4})}{A_R({}^5D_0 \rightarrow {}^7F_1)} = \frac{S({}^5D_0 \rightarrow {}^7F_{2,4})}{S({}^5D_0 \rightarrow {}^7F_1)} \qquad (1)$$

where

$$A_R({}^5D_0 \rightarrow {}^7F_2) = \frac{64\pi^4 e^2 \nu^3}{3h(2J+1)} \left(\frac{n(n^2+2)^2}{9}\right) \Omega_2 |\langle {}^5D_0 \| U^{(2)} \| {}^7F_2 \rangle|^2$$

$$A_R({}^5D_0 \rightarrow {}^7F_4) = \frac{64\pi^4 e^2 \nu^3}{3h(2J+1)} \left(\frac{n(n^2+2)^2}{9}\right) \Omega_4 |\langle {}^5D_0 \| U^{(4)} \| {}^7F_4 \rangle|^2$$

e is the electron's charge, ν is the energy of a transition (in cm^{-1}), h is the Planck's constant, n is the refractive index, and $J = 0$ for the emitting ${}^5D_0$ state. The last two equations determine the radiative transition probabilities for the indicated transitions (only the terms with non-zero reduced matrix elements are included). From those two ratios given by eq. (1) one can easily estimate the Ω_2 and Ω_4 parameters. The ${}^5D_0$–${}^7F_1$ magnetic dipole transition radiative transition probability is needed to use eq. (1). According to Ref. 21), it has the value of 57.34 s^{-1} for the $50(NaPO_3)_6+10TeO_2+20AlF_3+19LiF+1Eu_2O_3$ glass with refractive index 1.591. Taking this value as a reference and with a well-known correction factor of $(n/1.591)^3$, which can be derived from the general equations for the magnetic dipole transition probability rates[23,24] (here $n = 2.49$ is the refractive index of anatase), the ${}^5D_0$–${}^7F_1$ magnetic dipole transition radiative transition probability in our samples was estimated to be 220 s^{-1}.

Such a method of evaluating the intensity parameters for Eu^{3+} (the Ω_6 parameter cannot be estimated in this case, since the matrix elements of the $||U^{(6)}||$ operator for the considered transitions are zero) is widely used (Refs. 20–24). Table 1 lists the Judd-Ofelt intensity parameters for each sample studied in the present work.

The branching ratio for the ${}^5D_0 \rightarrow {}^7F_2$ emission transition is more than 70% — this is the most probable transition for the radiative deactivation of the ${}^5D_0$ excited state.

The quantum efficiency can be estimated as the ratio of the experimental lifetime τ_{exp} (which also accounts for the non-radiative losses) to the calculated radiative lifetime τ_{calc} (which does not take into account non-radiative processes). Using the data from Table 1, it can be seen that the quantum efficiency of the studied samples decreases from 0.83–0.85 for the samples with low concentration of Eu^{3+} to the value of 0.63 for the sample with 10 at% of Eu^{3+}. Obviously, increase of the Eu^{3+} concentration enhances non-radiative losses due to the re-absorption and energy transfer processes between closely located impurity ions. Moreover, with increasing the Eu^{3+} concentration the branching ratio of the ${}^5D_0 \rightarrow {}^7F_2$ emission transition is slightly decreased, which indicates re-distribution of intensities between the most prominent bands in the emission spectra. Among the JO

Table 1 Intensity parameters, calculated and measured lifetimes of the $^5D_0$ level of Eu^{3+} and branching ratios of the $^5D_0 \rightarrow {}^7F_J$ ($J = 1, 2, 4$) emission transitions for the TiO_2 anatase nanopowders with varying concentration of Eu^{3+}.

Eu^{3+} concentration, at%	Intensity parameters, 10^{-20} cm^2		Lifetime (ms) of the $^5D_0$ level		Branching ratios (%) of transitions from the $^5D_0$ level to the $^7F_1$, $^7F_2$, $^7F_4$ states, correspondingly	Baricenters of the $^5D_0$ to $^7F_1$, $^7F_2$, $^7F_4$ transitions (cm^{-1})		
	Ω_2	Ω_4	τ_{calc}	τ_{exp}		$^7F_1$	$^7F_2$	$^7F_4$
0.1	8.70	3.36	0.47	0.39	10.35; 75.35; 14.31	16932	16164	14326
0.5	8.75	3.54	0.46	0.39	19.14; 75.08; 14.79	16876	16227	14333
1	8.49	4.29	0.46	0.38	10.06; 72.19; 17.75	16869	16219	14318
3	6.98	3.39	0.55	0.37	12.06; 71.11; 16.83	16876	16221	14329
5	7.48	4.03	0.51	0.35	11.13; 70.39; 18.48	16873	16218	14329
7	7.70	4.14	0.49	0.33	10.86; 70.61; 18.53	16867	16210	14324
10	7.69	4.19	0.49	0.31	10.86; 70.44; 18.70	16885	16211	14323

intensity parameters, the Ω_2 parameter depends on the local environment around the Eu^{3+} site and it is strongly affected by covalence between Eu^{3+} and ligand anions, whereas Ω_4 is related to the viscosity and rigidity of the host material, in which the impurity ions are situated. So, higher the value of Ω_2, stronger the covalence and lower the symmetry.[25,26] According to Kumar *et al.*,[27] the trend observed in the calculated JO intensity parameters shown in Table 1 ($\Omega_2 > \Omega_4$) demonstrates the covalence existing between the Eu^{3+} ion and ligands as well as the asymmetry around the metal ion site. The covalence is reduced when TiO_2 nanoparticles are doped with the high concentrations of Eu^{3+} ions (> 3 at%).

4. Conclusions

Details of synthesis and experimental studies of the TiO_2 anatase nanopowders doped with Eu^{3+} ions are reported in the present paper. Efficient red emission of the Eu^{3+} ions can be obtained on account of the $^5D_0 \rightarrow {}^7F_2$ emission transition. The calculations of the radiative lifetimes along with the estimations of the experimental total lifetime of the Eu^{3+} excited $^5D_0$ state allowed to evaluate the quantum efficiencies for the obtained samples, which is as high as about 0.83 for the samples with low Eu^{3+} concentration. The performed studies show the slightly (up to 1%) Eu^{3+}-doped TiO_2 anatase nanopowders to be perspective luminescent materials. For higher doping concentrations, covalency and quantum efficiency are decreased.

Acknowledgments

The authors acknowledge Prof. S. P. Ahrenkiel for TEM measurements. Željka Antić, Katarina Vuković and Miroslav D. Dramićanin acknowledge the financial support of the Ministry of Education and Science of the Republic of Serbia (Project no. 45020) and the support from the APV Provincial Secretariat for Science and Technological Development of the Republic of Serbia through project no. 114-451-1850/2014-03. Mikhail G. Brik acknowledges the financial support of the Marie Curie Initial Training Network LUMINET through grant agreement 316906, the Programme for the Foreign Experts offered by Chongqing University of Posts and Telecommunications, European Regional Development Fund (Centre of Excellence "Mesosystems: Theory and Applications", TK114) and Ministry of Education and Research of Estonia, Project PUT430.

REFERENCES

1) M. R. Hoffmann, S. T. Martin, W. Choi and D. W. Bahnemann: Chem. Rev. **95** (1995) 69–96.
2) U. Stafford, K. A. Gray and P. V. Kamat: Heterogen. Chem. Rev. **3** (1996) 77–104.
3) A. L. Linsebigler, G. Lu and J. T. Yates, Jr.: Chem. Rev. **95** (1995) 735–758.
4) A. O. Ibhadon and P. Fitzpatrick: Catalysts **3** (2013) 189–218.
5) B. O'Regan and M. Grätzel: Nature **353** (1991) 737–740.
6) X. Chen and S. S. Mao: Chem. Rev. **107** (2007) 2891–2959.
7) V. Kiisk, I. Sildos, S. Lange, V. Reedo, T. Tätte, M. Kirm and J. Aarik: Appl. Surf. Sci. **247** (2005) 412–417.
8) C. C. Ting, S. Y. Chen, W. F. Hsieh and H. Y. Lee: J. Appl. Phys. **90** (2001) 5564–5569.
9) R. Palomino-Merino, A. Conde-Gallardo, M. García-Rocha, I. Hernández-Calderón, V. Castaño and R. Rodríguez: Thin Solid Films **401** (2001) 118–123.
10) A. Conde-Gallardo, M. García-Rocha, R. Palomino-Merino, M. P. Velásquez-Quesada and I. Hernández-Calderón: Appl. Surf. Sci. **212–213** (2003) 583–588.
11) C. Urlacher and J. Mugnier: J. Raman. Spectrosc. **27** (1996) 785–792.
12) Ž. Antić, R. Krsmanović, M. G. Nikolić, M. Marinović-Cincović, M. Mitrić, S. Polizzi and M. D. Dramićanin: Mater. Chem. Phys. **135** (2012) 1064–1069.
13) W. Luo, R. Li, G. Liu, M. R. Antonio and X. Chen: J. Phys. Chem. C **112** (2008) 10370–10377.
14) Y. Liu, W. Luo, H. Zhu and X. Chen: J. Lumin. **131** (2011) 415–422.
15) L. Li, C. K. Tsung, Z. Yang, G. D. Stucky, L. D. Sun, J. F. Wang and C. H. Yan: Adv. Mater. **20** (2008) 903–908.
16) M. G. Nikolić, Ž. Antić, S. Ćulubrk, J. M. Nedeljković and M. D. Dramićanin: Sens. Actuators B Chem. **201** (2014) 46–50.
17) M. D. Dramićanin, Ž. Antić, S. Ćulubrk, S. P. Ahrenkiel and J. M. Nedeljković: Nanotechnology **25** (2014) 485501.
18) B. R. Judd: Phys. Rev. **127** (1962) 750–761.
19) G. S. Ofelt: J. Chem. Phys. **37** (1962) 511–520.
20) H. Ebendorff-Heidepriem and D. Ehrt: J. Non-Cryst. Solids **208** (1996) 205–216.
21) D. Uma Maheswari, J. S. Kumar, L. R. Moorthy, K. Jang and M. Jayasimhadri: Physica B **403** (2008) 1690–1694.
22) R. Balda, J. Fernandez, J. L. Adam and M. A. Arriandiaga: Phys. Rev. B **54** (1996) 12076–12086.
23) J. C. Boyer, F. Vetrone, J. A. Capobianco, A. Speghini and M. Bettinelli: J. Phys. Chem. B **108** (2004) 20137–20143.
24) C. Liu, J. Liu and K. Dou: J. Phys. Chem. B **110** (2006) 20277–20281.
25) C. Koeppen, S. Yamada, G. Jiang, A. F. Garito and L. R. Dalton: J. Opt. Soc. Am. B **14** (1997) 155–162.
26) S. S. Braga, R. A. Saferreira, I. S. Goncalves, M. Pillinger and J. Rocha: J. Phys. Chem. B **106** (2002) 11430–11437.
27) M. Kumar, T. K. Seshagiri and S. V. Godbole: Physica B **410** (2013) 141–146.